

Thermomechanical fatigue life of a TBC – comparison of computed and measured behaviour of delamination cracks

Sören Sjöström^{1,*}, Håkan Brodin^{1,2}, Magnus Jinnestrand¹

¹ Department of Management and Engineering, Linköping University, SE-58183 Linköping, Sweden

² Siemens Industrial Turbomachinery AB, SE-61283 Finspång, Sweden

* Corresponding author: email@address.aa.b.cc

Abstract Thermal barrier coatings (TBCs) are used in hot parts of gas-turbine engines in order to increase gas temperatures and improve thermal efficiency. A TBC consists of a metallic bond coat (BC) and a ceramic top coat (TC).

During high-temperature service, thermally grown oxide will form in the BC/TC interface. This together with the general difference in mechanical and thermal expansion properties leads to a tendency of spalling damage, by which areas of the coating will flake off during thermomechanical cycling.

The modelling of this damage process is rather difficult, but the authors have managed to set up a fracture-mechanically based model, which takes thermal cycling, mechanical cycling and oxide growth into account. The model has been tested and verified under controlled laboratory conditions, using thermal cycling furnaces and continuous inspection of damage development. It has also been used in an FEM computation environment for prediction of TBC spalling in real gas-turbine components.

In this article, the model is described, computations are shown of the development of a typical delamination crack in the BC/TC interface, and the computed results are compared with actual delamination crack behaviour seen in the corresponding testing.

Keywords TBC, fracture-mechanical model, experimental, FEM, interface crack

1. Introduction

A thermal barrier coating (TBC) is a ceramic coating applied for thermal insulation purposes on a metallic substrate.

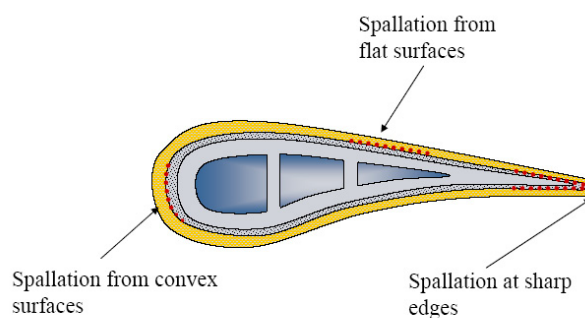


Figure 1. Schematic figure of a TBC-coated gas-turbine blade. Typical spalling mechanisms marked are explained below

Fig. 1 shows a schematic example of a TBC-coated gas-turbine blade. The TBC consists of a substrate (light grey in Fig. 1) on which a metallic bond coat (darker grey in Fig. 1) is applied. On top of the bond coat, finally, the top coat ceramic (yellow in Fig. 1) is applied. The substrate is usually a nickel-based superalloy, the bond coat is an alloy, rich in Al, and the top coat ceramic is usually

ZrO₂ with an addition of 6 à 8% Y₂O₃. . The purpose of the bond coat is to improve the adhesion and to prevent the oxidation by itself forming a dense oxide with as good mechanical properties as possible..

In the typical gas-turbine application, such components will be loaded by the thermomechanical start/stop cycle, *i.e.*, a start, followed by a full-load high-temperature period of from a couple of hours up to several days, finally followed by a shut-down. The design life requirements between inspections for a land-based gas turbine can typically be 3 000 cycles and 30 000 full-load high-temperature hours, after which the TBC must still be functional.

This document deals with air-plasma-sprayed (APS) TBC, which is the type most commonly used in stationary gas turbines.

2. TBC fatigue life

Thermomechanical fatigue (TMF) aspects. Experience shows that with time (and, consequently, accumulated load cycles) TBCs are prone to failing by spalling (flaking). The most dangerous spalling mechanisms have been shown to appear at the end of the shutdown after a long high-temperature full-load period. At the end of the high-temperature full-load period, the stress state in the interface-near region will be low due to high-temperature creep, and as the top coat (ceramic) has a much lower thermal expansion than the metallic layers below, the top coat will be in strong compression at the end of the shut-down (at ‘room temperature’). This leads to the three main spalling mechanisms illustrated in Fig. 1.

Of the spalling mechanisms shown in the figure, most research has been concentrated on the explanation and analysis of the spalling from flat surfaces.

TBC life models: history and present status. Early research (see, for instance, [1]) showed that the geometry of the interface (which has a pattern of repeated ridges and valleys caused by the plasma-spray process) leads to tensile stress normal to the interface during the stop cycle of the gas turbine, so that the initiation and growth of cracks in the interface is made possible. Similar analyses on an improved 3-D FE model in [2] confirmed this mechanism. This insight led us to the set-up of a fracture-mechanically based life model

3. Fracture-mechanical model of a TBC

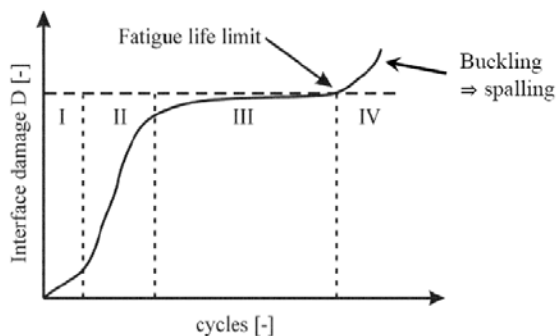


Figure 2. Measured damage evolution in APS TBC

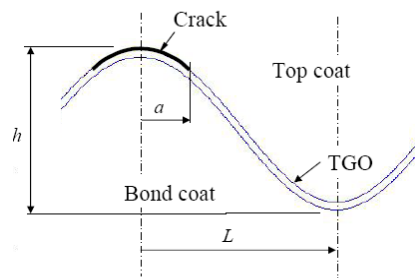


Figure 3. Idealised interface/crack geometry for the FM model

For the fracture-mechanical computations, a least representative cell has been defined, consisting of a substrate+bond coat+TGO+top coat cell, having the width L (= half the period of the idealised cosine wave of Fig. 3). This cell has been given boundary conditions corresponding to symmetry along the left-hand vertical boundary.

The model bases on an idealised (sinusoidal) bond coat (BC)/top coat (TC) interface profile, in which the thermally grown oxide (TGO) is assumed to grow. See Fig. 3. Equal cracks grow symmetrically from all profile tops, *i.e.*, when $D = a/L = 1.0$, cracks extend along the whole interface, leading to complete failure. Further essential model assumptions:

- Plane strain
- Stress-free TBC system at the end of the high-temperature part of the cycle
- The maximum damage-driving energy release rate G and stress intensity factors K_I and K_{II} appear after cooling down from the maximum temperature (low thermal expansion of the TC)
- The material behaviour of all components of the TBC aggregate during the cooling down from maximum temperature is assumed to be linearly elastic

G , K_I and K_{II} are computed by a virtual crack extension method and by interface crack theory (see [3] and appendix)

Fig 4 shows examples of the FE geometry and of the stress pattern in the interface region for 4 typical h/L cases

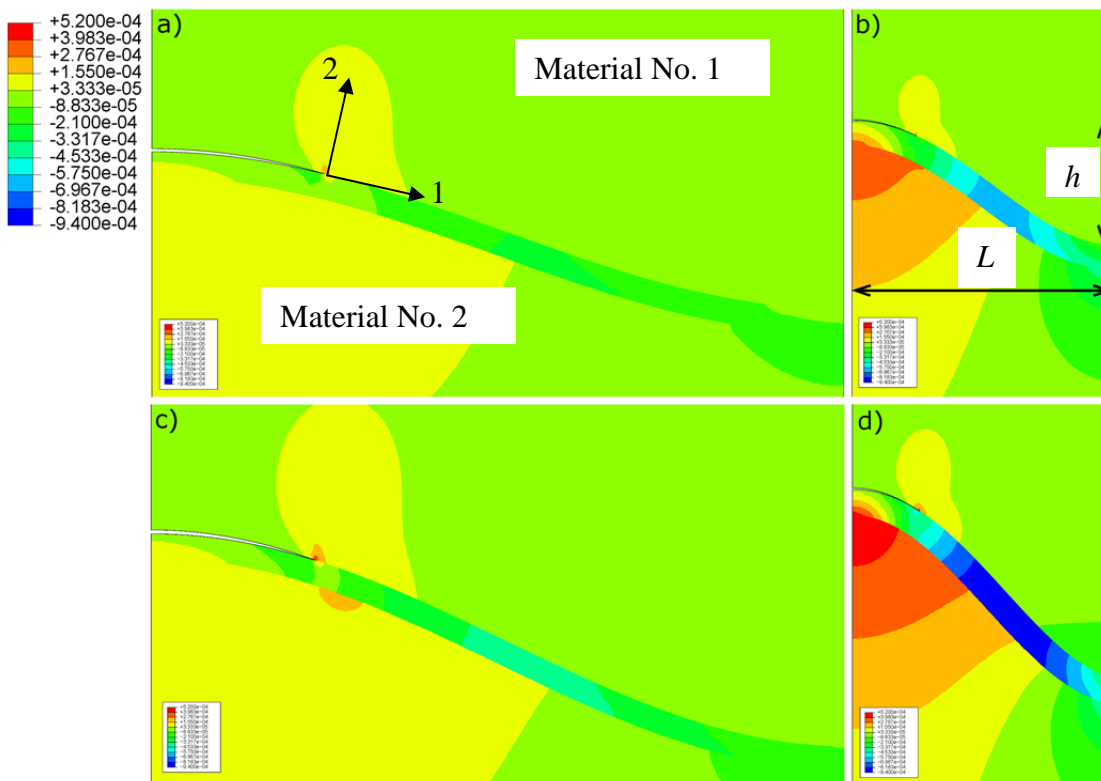


Figure 4. Examples of the FE geometry and of the stress pattern in the interface region for 4 typical h/L cases.

Most of the FE computations so far have been done in an in-house code. We have, however, moved over to the commercial code Abaqus for a planned continuation, which will, among other things, in-

involve creep modelling of the bond coat.

G , K_I and K_{II} have been computed for different h/L , different δ_{TGO} and continuously increasing crack lengths corresponding to damage $D_m = a/L$ in the interval $0.0 < D_m < 1.0$. See examples in Fig.5.

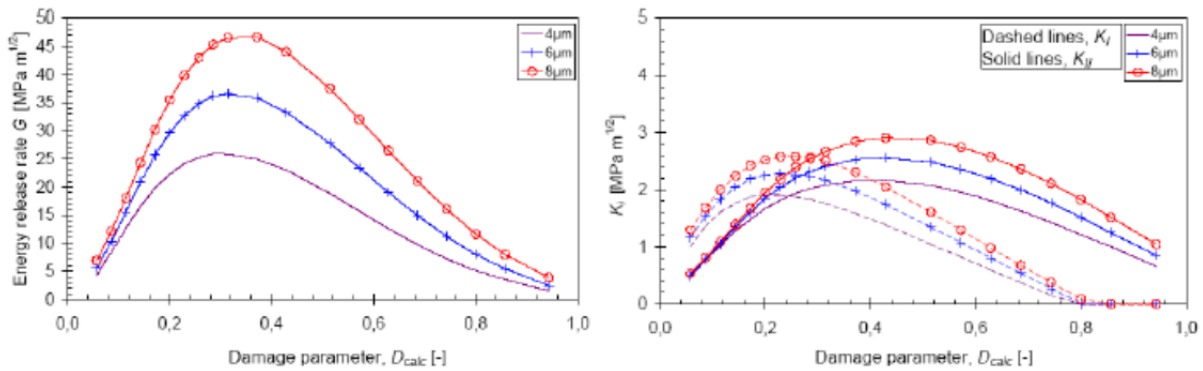


Figure 5. Energy release rate G and stress intensity factors K_I and K_{II} computed for the TCF test.

4. Experimental details

An experimental study has been conducted with the aim at giving quantitative data on crack propagation at a ceramic / metal interface. Evaluations are done on thermally cycled material and material exposed to engine conditions. The coatings evaluated are thin thermal barrier NiCoCrAlY coatings, with nominal thicknesses of top coat equal to $300\mu\text{m}$ and bond coat thickness of $150\mu\text{m}$.

Thermal cycling is performed in air with furnace heating and cooling by forced air. The furnace cycling consists of a standard cycle type where small coupons $30 \times 50 \times 5$ mm are exposed to a thermal cycle with 60 minutes dwell time in the furnace at constant temperature. Heating and cooling parts of the cycle are 10 minutes respectively. Data have been retrieved for interrupted tests where the cycling has been stopped after approximately 30% of the expected fatigue. Ex-serviced material has been included with corresponding conditions, i.e. 30-40% of the expected service life.

Coating infiltration by epoxy ensures that the exposed microstructure is retained and that the structure studied is not an artifact after sample preparation. After the epoxy infiltration, the material is cut and mounted for grinding and final polishing. All evaluations are done on as polished cross sections.

Cracks at the top coat / bond coat interface are identified and measured. Measurements are registered for the general microstructure geometry in regions where isolated defects are detected, see Figure 6. In Figure 6 the typical microstructure TBC is shown (a). The interface is undulating and a least representative cell is not easily detected. Instead the morphology of individual undulations needs to be considered (b). The structure is necessarily not similar to the structure observed in the modeling approach (c). In general, the microstructure is assumed to be described with the height over width ratio as defined for modeling purposes.

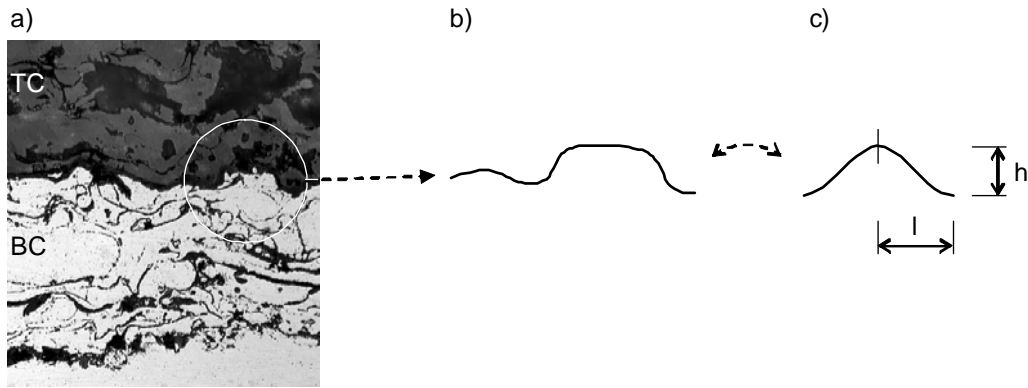


Figure 6. Comparison of interface microstructure / morphology in actual thermal barrier coatings.

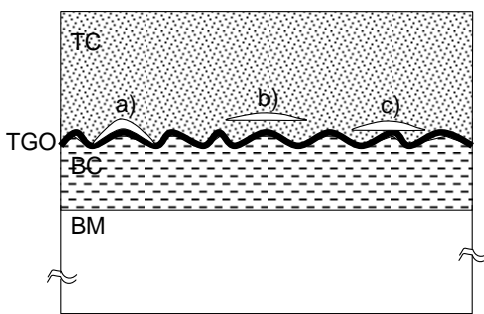


Figure 7. Crack patterns observed in thermal barrier coatings. (a) black interface crack, (b) ceramic white crack and (c) mixed black/white crack with the crack partly at the interface, partly in the top coat.

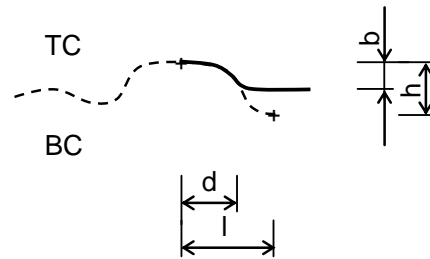


Figure 8. Definition of measurement on deflected kink crack.

Different crack types can theoretically be observed in the ceramic / metal material system. The three typical crack patterns are shown in **Error! Reference source not found.**. The different crack patterns (a), (b) and (c) are identified as black TC/BC interface cracks, white ceramic TC cracks and mixed kink cracks with portions of the crack both at the TC / BC interface as well as portions in the ceramic TC respectively. Cracks of type (c) are contained inside the TGO layer especially if the oxide is formed on an alloy with relatively low Al concentration. In such cases, the oxide is often observed to contain many defects and can be described as layered. During thermal fatigue exposure of the coatings, damages of type (a) are common. Also damage of type (c) is frequently observed after furnace testing and engine exposure. Damage of type (b) is not frequently occurring. This damage pattern is more related to high heat flux situations in burner test rigs and corresponding engine situations with high thermal loads

A schematic picture of the measurements taken is shown in **Error! Reference source not found.**. The measure d is defined as the distance from a ridge to the location where a crack deflects away from the interface into the top coat projected on a plane parallel to the interface (and the TBC outer surface). Also the distance vertically (perpendicular) from the ridge to the location of crack deflection is measured, in **Error! Reference source not found.** defined as b .

At the location of crack deflection from interface to TC crack the curve shape tangent dy/dx , or curve shape first derivative, is measured (a). On the corresponding model, the curvature has been described by a tangent as shown in (b) and (c). The tangent (b) is the slope at the inflexion point

with the highest value of dy/dx . This is to be compared to the average dy/dx value measured as the measure peak-to-valley over half wavelength, i.e. h/l .

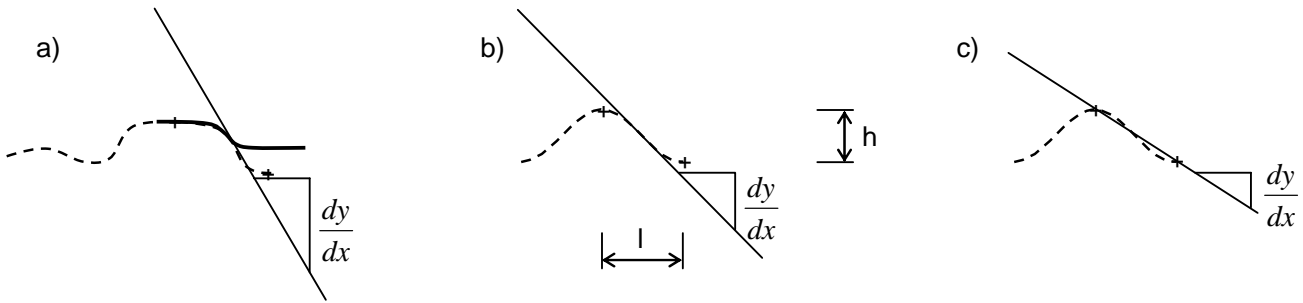


Figure 9. Definition of measurements for determination of angle for crack deflection. Figure (a) represents a real interface, (b) measurement of maximum slope for theoretical sinusoidal interface and (c) measurement of average slope for theoretical sinusoidal interface.

5. Comparison of fracture-mechanical model results and microstructural damage evolution

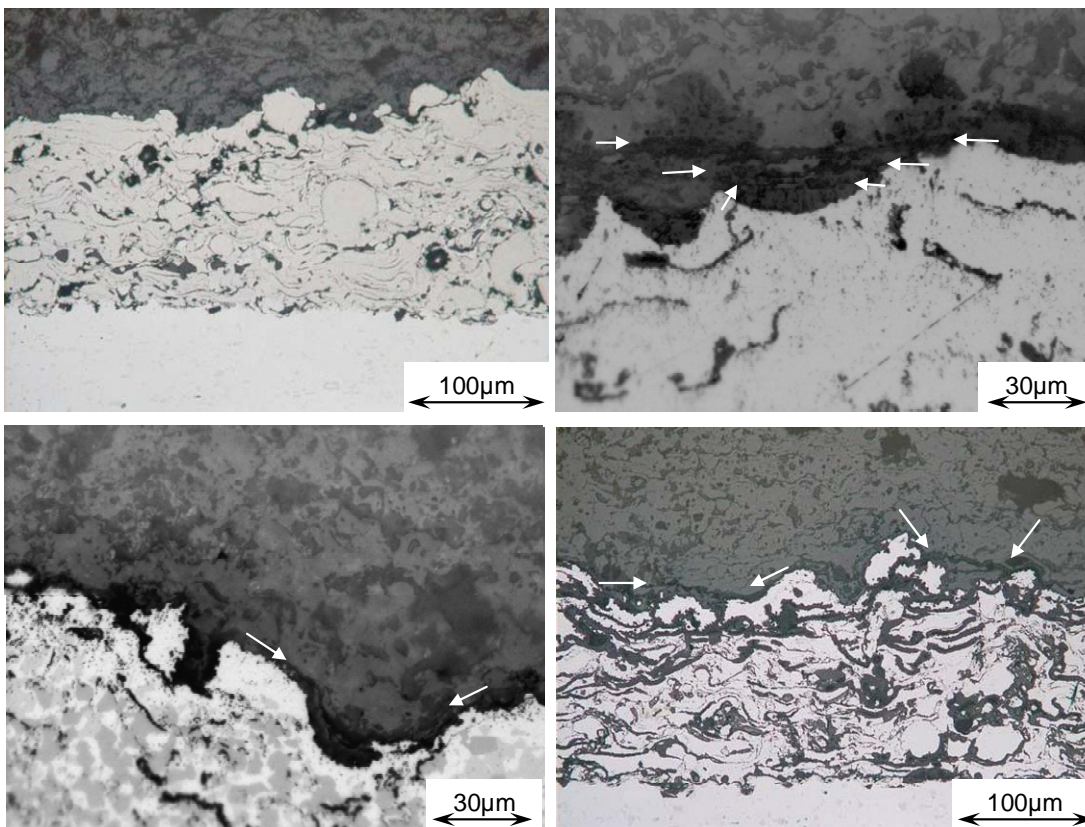


Figure 10. Typical microstructures of virgin (a) and ex-serviced materials (b) – (d). Multiple kink cracks (b) interface crack (c) and kink/white cracks after furnace testing (d).

Examinations of thermally cycled material (furnace and engine exposed) reveal that the material damage is similar. To a large extent the material damage is of interface type (black) but mixed cracking (black/white kink cracks) is frequently detected. Typical microstructures are shown in Figure 10. Image (a) is as manufactured, (b) and (d) indicate mixed (kink) deflected cracks from

furnace-cycled and engine-exposed, respectively. An interface crack formed during furnace cycling is shown in image (c).

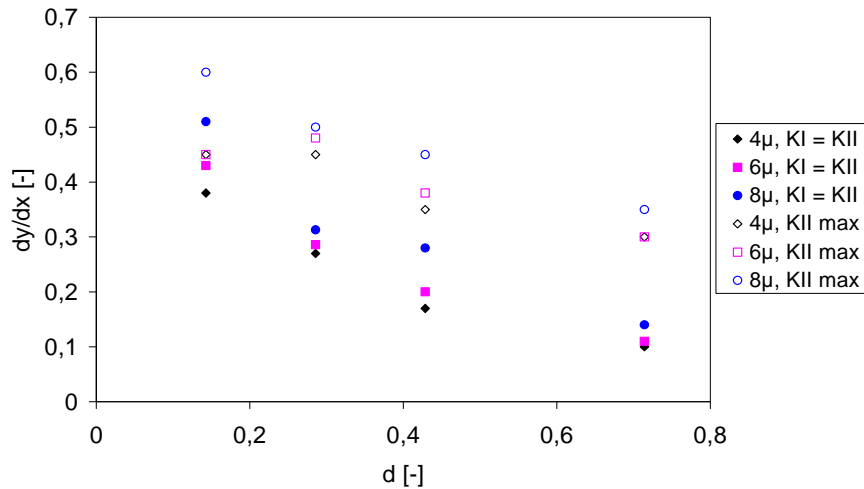


Figure 11. Correlation $dy/dx = f(D, K_I = K_{II})$ and $D = f(K_{II\ max})$.

From the data in Figure 5 the damage level D for $K_I = K_{II}$ and maximum K_{II} are determined. These data are presented in Figure 11. Data in Figure 11 are for interface roughness 10/70, 20/70, 30/70 and 50/70 $\mu\text{m}/\mu\text{m}$. Series are included for a range of oxide thickness values.

For individual kink cracks data are collected for peak-to-valley h , half-wavelength l , distance b and d for crack deflection and interface slope dy/dx at location for crack deflection.

Data indicate that the actual location for crack deflection from an interface crack to a deflected kink crack best can be described by a correlation of peak to location for deflection b along the surface normal rather than the projection on a plane parallel to the interface. It is also obvious that the condition for crack deflection best is described by a correlation to the maximum slope of the generalised model interface.

Results according to Figure 13 should be interpreted with the stress state at the interface in mind. For short cracks, the stress state is K_I dominated. As the crack progresses, the stress state will be increased dominated by shear stresses. Considering crack growth in an isotropic material, the general assumption is that a crack growing in a mixed mode stress field will try to grow in the direction that enables growth under a K_I modus. In the case of crack growth at a biomaterial interface, this is not necessarily true. A crack can continue to grow at the interface, if, for instance, the interface acts a weak link. An example of this is the TBC system with a thick thermally grown oxide that acts as a prescribed crack path. In cases where the thermally grown oxide is dense and adherent to the underlying metallic material, the crack should, in principle, be able to deflect away from the interface and into the top coat where crack growth can take place under a K_I dominated stress field. Figure 14 visualises the criterion that can be used to determine when the crack should have possibility to deflect into the top coat. For short cracks and low stress intensities, the crack is confined to the interface. As the crack grows longer and the interface oxidizes, the shear stress increases and the conditions for crack deflection can be fulfilled at $D=D_m$. It is important to notice that not all cracks will deflect. One important factor can be local TGO growth. It is well-known that the oxide thickness is not constant throughout a thermally exposed TBC coating even if the temperature is known and constant over the coating at T_{max} .

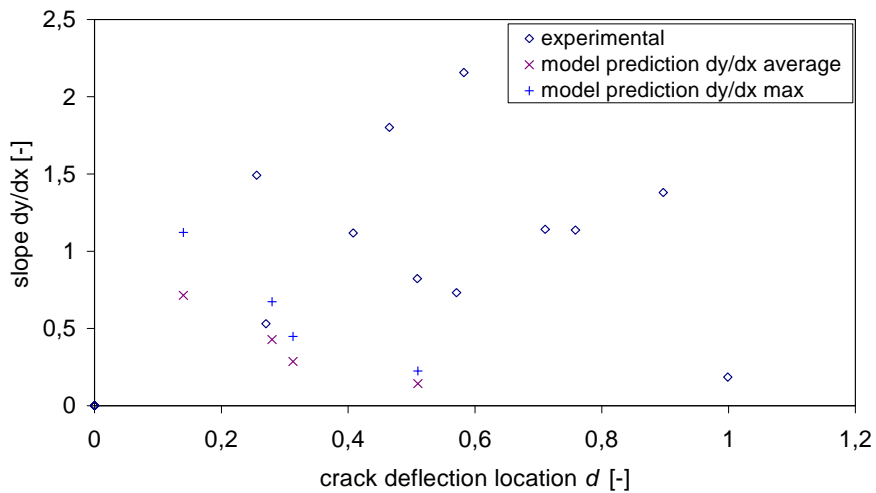


Figure 12. a) Correlation $dy/dx = f(d)$ and $dy/dx_{average} = d(K_I = K_{II})$ for experimental data and model results. b) Correlation $dy/dx = f(d)$ and $dy/dx_{max} = d(K_I = K_{II})$ for experimental data and model results.

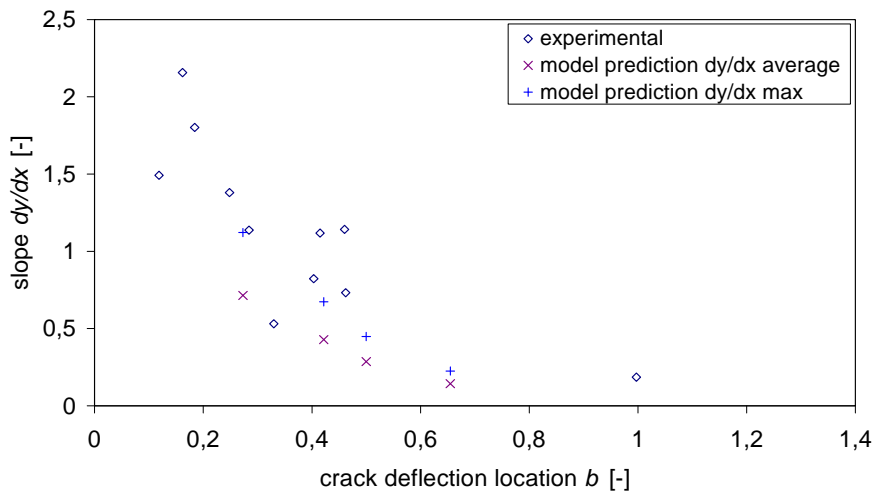


Figure 13. Correlation $dy/dx = f(b)$ and $dy/dx_{average} = b(K_I = K_{II})$ for experimental data and model results. b) Correlation $dy/dx = f(b)$ and $dy/dx_{max} = b(K_I = K_{II})$ for experimental data and model results.

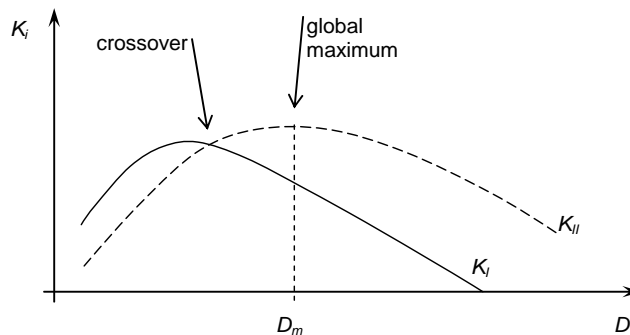


Figure 14. Possible criteria for change from interface crack to kink crack.

To some extent, the model tends to underestimate the slope required for transfer from mixed mode crack growth over to crack growth under a K_I dominated stress state. Hence, it can be argued that the stress state is overestimated at the interface. From these facts the conclusion could be that the

stress state determined by an FE-model is in the correct order of magnitude, and that the location for crack deflection can be described by $K_{II\ MAX}$ correlated to interface slope. However, it is likely that the stress level should be subject to further investigation. If $K_{II\ MAX}$ can be used as a criterion for crack deflection and the model prescribes this phenomenon to occur prematurely, the material response causes stresses to be exaggerated. Factors that can play a role in the mathematical modelling can be top coat stiffness, interface geometry, BC constitutive model, oxidation behaviour and thermal/mechanical load.

6. Conclusions

The current paper compares experimental findings and modelling results coupled to conditions for when a TBC delamination will change from an interface crack to a kink crack contained partly at the interface, partly in the ceramic top coat. It is shown that the condition for change from interface to kink crack can be fulfilled by comparison of interface slope and interface geometry in terms of asperity height. Comparisons indicate that the interface slope plays an important role and that experimental and modelling results correlate if the distance from peak to deflection point is taken into consideration. In the comparison, modelling results give the best agreement if the location for $K_{II\ max}$ is chosen as a criterion for when deflection is to be expected.

References

- [1] G.C. Chang, W. Phucharoen, Behavior of thermal barrier coatings for advanced gas turbine blades, Surf. and Coat. Techn. 30 (1987) 33-38
- [2] J.M. Jinnestrand, S. Sjöström, Investigation by 3D FE simulations of delamination crack initiation in TBC caused by alumina growth, Surf. and Coat. Techn. 135 (2001) 188-195
- [3] J.W. Hutchinson, Z. Suo, Mixed mode cracking in layered materials, Adv. Appl. Mech. 29 (1990). 63-187

Appendix: Mechanics of the interface crack

For a description of the theory of an interface crack see, for instance, [3].

From the FE solution, the energy release rate G and the crack flank displacements $u_1^{(u)}$, $u_1^{(l)}$, $u_2^{(u)}$ and $u_2^{(l)}$ at a number of nodes along the crack flank are used. (For definition of materials Nos. 1 and 2 and coordinate directions 1 and 2, see Fig. 4.)

The relation between G , K_I and K_{II} is given by

$$G = \left(\frac{1}{E_1^*} + \frac{1}{E_2^*} \right) \cdot \frac{1}{2 \cosh^2(\pi\epsilon)} (K_I^2 + K_{II}^2) \quad (1)$$

in which

$$\epsilon = \frac{1}{2\pi} \ln \frac{\frac{1+\nu_2}{E_2} + \kappa_1 \frac{1+\nu_1}{E_1}}{\kappa_2 \frac{1+\nu_2}{E_2} + \frac{1+\nu_1}{E_1}} \quad (2)$$

$$\kappa_i = \begin{cases} 3 - 4\nu_i; & \text{plane strain} \\ \frac{3 - \nu_i}{1 + \nu_i}; & \text{plane stress} \end{cases} ; i = 1,2 \quad (3)$$

$$E_i^* = \begin{cases} \frac{E_i}{1 - \nu_i^2} ; \text{plane strain} \\ E_i ; \text{plane stress} \end{cases} ; i = 1, 2 \quad (4)$$

Using the general fracture-mechanical solution for an interface crack, $\delta_1 = u_1^{(u)} - u_1^{(l)}$ and $\delta_2 = u_2^{(u)} - u_2^{(l)}$ (where superscripts (u) and (l) stand for upper and lower crack flanks, respectively) are then given by

$$\begin{bmatrix} \delta_1 \\ \delta_2 \end{bmatrix} = \Psi \cdot \begin{bmatrix} \sin(\epsilon \ln r) - 2\epsilon \cos(\epsilon \ln r) & 2\epsilon \sin(\epsilon \ln r) + \cos(\epsilon \ln r) \\ 2\epsilon \sin(\epsilon \ln r) + \cos(\epsilon \ln r) & -\sin(\epsilon \ln r) + 2\epsilon \cos(\epsilon \ln r) \end{bmatrix} \begin{bmatrix} K_I \\ K_{II} \end{bmatrix} \quad (5)$$

where

$$\Psi = \frac{1}{2} \left(\frac{1}{E_1^*} + \frac{1}{E_2^*} \right) \cdot \frac{8}{(1 + 4\epsilon^2) \cosh(\pi\epsilon)} \cdot \left(\frac{r}{2\pi} \right)^{\frac{1}{2}} \quad (6)$$

Eq. (6) is only used for establishing an expression for $\beta = K_I/K_{II}$:

$$\beta = \frac{K_I}{K_{II}} = \frac{-[\sin(\epsilon \ln r) - 2\epsilon \cos(\epsilon \ln r)] \cdot \delta_1 - [2\epsilon \sin(\epsilon \ln r) + \cos(\epsilon \ln r)] \cdot \delta_2}{-[2\epsilon \sin(\epsilon \ln r) + \cos(\epsilon \ln r)] \cdot \delta_1 + [\sin(\epsilon \ln r) - 2\epsilon \cos(\epsilon \ln r)] \cdot \delta_2} \quad (7)$$

In order to improve numerical performance, this computation of β is done for a number of positions along the crack, and the average of these is used together with Eq. (1) for the final computation of K_I and K_{II} :

$$\begin{cases} K_I = \sqrt{\frac{GH}{1 + \frac{1}{\beta^2}}} \\ K_{II} = \sqrt{\frac{GH}{1 + \beta^2}} \end{cases} \quad (8)$$